Soft Matter

PAPER

View Article Online
View Journal



Cite this: DOI: 10.1039/d4sm00903g

# Effect of cosolvents on the phase separation of polyelectrolyte complexes†

Yuanchi Ma, *[a] Robert J. S. Ivancic, [b] Jan Obrzut,[b] Debra J. Audus [b] and Vivek M. Prabhu *[b]

Received 27th July 2024,
Accepted 3rd September 2024

DOI: 10.1039/d4sm00903g

rsc.li/soft-matter-journal

Evidence is shown that cosolvent mixtures control the coacervation of mixtures of oppositely charged polyelectrolytes. Binary and ternary solvent mixtures lead to non-monotonic solubility as a function of the average dielectric constants of the solvent mixtures. These data are rationalized by considering both electrostatic-driven phase separation and solvophobic-driven phase separation using group contribution effects on solubility parameters. These estimates are introduced into an effective Flory–Huggins interaction parameter within the framework of Voorn–Overbeek theory with variable dielectric constants and temperature dependences. Despite its simplicity, the model recovers salient experimental observations not only on their coacervate stabilities, but also on their lower critical solution temperature behaviors. These observations highlight the importance of weak van der Waals interactions in determining the phase behaviors of polyelectrolyte complexes relative to electrostatic correlations.

## Introduction

Associative phase separation is a common phenomenon in polyelectrolyte complexes (PECs), whereby oppositely charged polyelectrolytes separate into solvent-rich supernatant phases and polymer-rich coacervate phases. Despite their broad applications in adhesives,[1,2] structured membranes, coatings[3] and therapeutic delivery vehicles,[4] a comprehensive physical picture of PECs needs to be elucidated. The convolution between the long-range electrostatic and van der Waals interactions in multicomponent systems adds to the challenge to model experimental data.[5] The relative significance of these two classes of interactions is debated across a variety of systems, including ionic fluids,[6–8] polyelectrolyte brushes,[9,10] and intrinsically disordered proteins.[11] In PECs, the role of charge correlation is increasingly invoked as a major contributor to phase separation,[12] where the complexation of polyelectrolytes and the concomitant counterion release are driving forces.[13,14] Nonetheless, in the literature, polyelectrolyte complexes have hitherto been discussed almost exclusively in aqueous media, whereas experiments and theories on PECs in binary and more complicated solvent mixtures are largely unexplored.

Similar to neutral polymer solutions, polyelectrolyte complex solutions also display unique critical temperature behaviors.[15–17] Their net temperature dependences are governed primarily by a static dielectric constant ($\varepsilon_0$) and an effective Flory–Huggins parameter ($\chi$). The former is embodied within the Bjerrum length ($l_B$) that equates the thermal energy to the Coulombic potential energy between charges separated in a dielectric medium. The latter is the sum of all enthalpic contributions to the mixing free energy, arising from the weak van der Waals interactions between nearest neighbors, such as monomers and solvent molecules, often referred to as the "solvophobic" contribution. It was reported that synthetic PECs in aqueous solution primarily display lower critical solution temperature (LCST) behavior,[18,19] whereas upper-critical solution temperature (UCST)[20] is occasionally observed. Such critical temperature dependences were successfully modelled by Adhikari *et al.*[21,22] using the combinations of realistic temperature ($T$) dependencies of $\varepsilon_0$ and two empirical $\chi(T)$ functions to differentiate electrostatic and the solvophobic contributions to the phase separation of PECs. Notably, in their computation, LCST, UCST and both LCST and UCST behaviors are predicted depending on the exact parameterization, suggesting the complexity of such systems. Similarly, Ylitalo *et al.*[23] showed that the LCST was electrostatic in origin by considering the temperature dependence of the dielectric constant in liquid state theory.

On the experimental side, attempts were made to deconvolute the effect of Coulombic interactions and van der Waals interactions on the coacervation of PEC solutions. Li *et al.* systematically studied two PECs with nearly identical charge density but distinct backbone–solvent interactions: the

[a] College of Polymer Science and Engineering, Qingdao University of Science and Technology, Qingdao, Shandong, China. E-mail: yuanchi.ma@qust.edu.cn
[b] Materials Science and Engineering Division, Material Measurement Laboratory, National Institute of Standards and Technology, 100 Bureau Drive, Gaithersburg, MD, USA. E-mail: vprabhu@nist.gov

† Electronic supplementary information (ESI) available. See DOI: https://doi.org/10.1039/d4sm00903g

hydrophobic pair comprises sodium poly(acrylate) (PAA) and poly(allylamine hydrochloride) (PAH) with aliphatic backbones, while the hydrophilic pair comprises poly(D,L-glutamic acid sodium salt) (PRE) and poly(L-lysine hydrochloride) (PLK) with peptide backbones. The former was shown to phase-separate more readily, than the cross-paired PAA + PLK and PRE + PAH, than the latter.[24] In an earlier study, Lou *et al.* started with a pair of hydrophobic, sulfide-containing poly(sulfonate) and poly(amine hydrochloride) and applied different oxidation levels to tune the backbone–solvent interactions while keeping the charge density nearly constant. They observed a clear downshift of the salt-dependent binodal phase envelopes with increasing oxidation levels (*i.e.*, backbone hydrophilicity).[25] Despite the chemical difference in PECs, both authors reported enhanced miscibility of the complexes when the backbone–solvent (water) interaction becomes more favorable, reminiscent of the phase behavior of simple binary mixtures of neutral polymers and solvents in the spirit of Flory–Huggins theory. Considering these previous studies, we sought to push our understanding one step further by keeping the PEC backbones constant while investigating the effect of varied solvent compositions to the phase behavior of PECs, where $\varepsilon_0$ and $\chi$ simultaneously changed by solvent compositions in a non-trivial way.

Potassium poly(styrene sulfonate) (KPSS) and poly(diallyldimethylammonium)bromide (PDADMAB) are two water soluble polyelectrolytes, while their complexation results in phase-separation under ambient temperature and low-salt conditions. With a charge stoichiometry of 1 : 1, the transition of this complex solution from two-phases to one-phase takes place at approximately 1.8 mol $L^{-1}$ of added KBr, defined as the salt resistance or the threshold salt concentration ($c_{s,th}$).[19,26,27] As $c_{s,th}$ depends on the total polyelectrolyte concentration[18,19] ($c_p$), it is therefore facile to use $c_{s,th}$ at a given $c_p$ as the proxy for the height of the two-phase window in the entire phase diagram. This strategy was employed previously[28–31] as a simple and intelligible way to report the phase behaviors of a variety of polyelectrolyte complex solutions. In this study, we fixed $c_p$ = 0.10 mol $L^{-1}$ and $T$ = 20 °C, while varying the volume fraction of cosolvents and the total salt concentration ($c_s = c_{s,added} + c_{s,counterion}$) progressively to determine the $c_{s,th}$ for each solvent composition. We selected ethylene glycol (EG) and *N*-methylformamide (NMF) as the cosolvents, as they are both miscible with water and have moderate solubilities to the two polyelectrolytes and the salt (KBr). Furthermore, pure EG has a lower static dielectric constant ($\varepsilon_{EG}$ = 38) than water ($\varepsilon_{H_2O}$ = 80) at room temperature, while pure NMF has a much higher static dielectric constant ($\varepsilon_{NMF}$ = 187) partially due to the presence of directional hydrogen bonds.[32,33] Therefore, mixing EG or NMF with water allows for the tuning of a wide range of static dielectric constants and consequently the strength of electrostatic interactions. Previous fundamental research on the temperature-dependence of low ionic strength polyelectrolytes in NMF solutions was the first to study the effect of varied Bjerrum length on the dynamics.[34–36]

# Results and discussion

### Phase behavior of PECs at various solvent compositions

The phase behaviors of the KPSS–PDADMAB complexes were investigated in binary and ternary solvent mixtures of $H_2O$ with EG and NMF for cosolvent volume fractions relative to the solvent volume ($\varphi^S_{EG}$ and $\varphi^S_{NMF}$) up to 0.50 (Table 1). The upper bound of the cosolvents is restricted by the solubility of the polyelectrolytes and KBr; therefore, the regions of $\varphi^S_{EG} + \varphi^S_{NMF} > 0.5$ were not further pursued. We conducted broadband dielectric spectroscopy measurements to determine the $\varepsilon_0$ of each solvent mixture (see the Experimental section and Section I of the ESI† for more details). These measurements agree with the literature values.[32,33,37] By plotting the data in Table 1 with $c_{s,th}$ against $\varepsilon_0$ (as shown in Fig. 1a), for the binary solvent mixtures (EG + $H_2O$ in blue and NMF + $H_2O$ in red), $c_{s,th}$ does not show monotonic dependence on $\varepsilon_0$, but display a sharp maximum at $\varepsilon_0$ = 80 (the black symbol), corresponding to the case of water. From the perspective of solvent compositions, most of the variance in $c_{s,th}$ can be qualitatively explained by the volume fraction of water $\left(\varphi^S_{H_2O}\right)$, regardless of the direction of $\varepsilon_0$. A similar trend is evident in ternary solvent mixtures with varying $\varphi^S_{H_2O}$ and constant ratio of $\varphi^S_{EG}/\varphi^S_{NMF}$ (the green symbols). On the high dielectric constant branch (NMF + $H_2O$), this trend is expected because the strength of electrostatic interactions decreases with $\varepsilon_0$, leading to the enhanced stability of soluble complexes, and therefore lower salt concentration required to homogenize the system. On the low dielectric constant branch (EG + $H_2O$), however, we note that the decreased $c_{s,th}$ at lower $\varepsilon_0$ (or higher Bjerrum length $l_B$) is in contrast with predictions by Zhang *et al.* using a $\chi$-free model based on liquid-state theory,[38] but in agreement with a recent experimental work by Meng *et al.*,[39] who also observed decreased $c_{s,th}$ for PSS-PVBTMA [poly(vinylbenzyl)trimethylammonium chloride] complexes under lower dielectric conditions in water–ethanol mixtures, where the static dielectric constant of ethanol is 24.5. These strongly suggest

Table 1 $c_{s,th}$ of KPSS–PDADMAB complexes in solvent mixtures at $c_p$ = 0.10 mol $L^{-1}$

| Solvent | $\varphi^S_{H_2O}$ | $\varphi^S_{EG}$ | $\varphi^S_{NMF}$ | $\varepsilon_0$[a] | $c_{s,th}$ [mol $L^{-1}$] |
|---|---|---|---|---|---|
| $H_2O$ | 1.00 | 0 | 0 | 80.0 | 1.80 ± 0.01 |
| Binary: $H_2O$/EG | 0.90 | 0.10 | 0 | 76.8 | 1.59 ± 0.01 |
| | 0.75 | 0.25 | 0 | 71.6 | 1.35 ± 0.01 |
| | 0.60 | 0.40 | 0 | 66.5 | 1.14 ± 0.01 |
| | 0.50 | 0.50 | 0 | 62.7 | 1.10 ± 0.01 |
| Binary: $H_2O$/NMF | 0.90 | 0 | 0.10 | 83.2 | 1.41 ± 0.01 |
| | 0.75 | 0 | 0.25 | 88.0 | 1.20 ± 0.01 |
| | 0.60 | 0 | 0.40 | 95.3 | 1.05 ± 0.01 |
| | 0.50 | 0 | 0.50 | 102.1 | 1.00 ± 0.01 |
| Ternary: $H_2O$/EG/NMF | 0.90 | 0.072 | 0.028 | 78 ± 1[b] | 1.52 ± 0.01 |
| | 0.75 | 0.18 | 0.07 | 75.0 | 1.27 ± 0.01 |
| | 0.60 | 0.288 | 0.112 | 70 ± 1[b] | 1.09 ± 0.01 |
| | 0.50 | 0.36 | 0.14 | 68.0 | 1.05 ± 0.01 |

Note: [a] Measured by dielectric spectroscopy. [b] Calculated by interpolation of the experimental data.

 

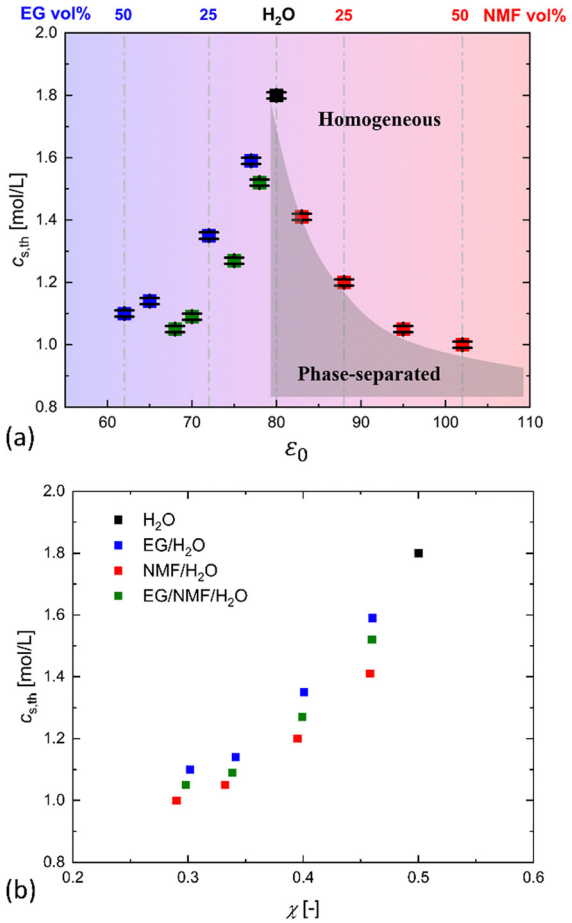


Fig. 1 (a) $c_{s,th}$ of KPSS–PDADMAB complexes as a function of $\varepsilon_0$ (bottom axis). The blue and red symbols represent the binary mixtures of EG + $H_2O$ and NMF + $H_2O$, respectively; the green symbols represent the ternary mixtures. The dash-dotted lines indicate the solvent compositions (top axis) and the grey-shaded area reminds readers of the phase-separated nature of PECs in the low-salt regime. These marks are for visual aid only. (b) The same data in (a) plotted as a function of $\chi_{avg}$ (see Table 2 and related narrative for details). Uncertainties were not estimated for values of $\chi$.

the importance of invoking an effective $\chi$ to account for the discrepancy between theories and experiments.

By its strict definition, $\chi$ of a binary mixture should only reflect the overall local enthalpic interactions. In multicomponent ion containing systems such as polyelectrolytes and PEC solutions, the solution may require multiple $\chi$'s to account for all pair-wise interactions or an effective $\chi$ that assumes a lumped contribution. Therefore, in the present study, we seek to estimate the $\chi$ between solvents and polyelectrolytes ($\chi_{solvent\text{-}p}$) through the group contribution theory based on Hansen solubility parameters,[40,41] a classical approach to predict the miscibility of neutral compounds. The equivalent uncharged structures for $PSS^-$ and $PDADMA^+$ are proposed in Scheme S1 (ESI†), and a short account of this approach is given in the ESI.† The results of these calculations are given in Table 2. These values are computed with respect to the reference volume $l^3 = 0.0366\ nm^3$ and scaled to provide reasonable agreement between our theoretical model and experimental results. While the scaling parameter is somewhat less than the optimal one found in ref. 42, we note that much of the previous study's data were fit to poly(butyl methacrylate) and poly(vinyl acetate). On average, the Flory–Huggins parameters between the pure solvents and the equivalent polyelectrolyte pairs, *i.e.*, $\chi_{H_2O\text{-}p}$, $\chi_{EG\text{-}p}$ and $\chi_{NMF\text{-}p}$ are 0.50, 0.10 and 0.080, respectively. These values are estimates of the charge-deconvoluted solvent–polymer interactions as both the polyanion and the polycation have hydrophobic backbones, and their solvent selectivity should follow the order of increasing hydrophobicity, *i.e.*, $H_2O < EG < NMF$, which naturally leads to $\chi_{H_2O\text{-}p} > \chi_{EG\text{-}p} > \chi_{NMF\text{-}p}$. Fig. 1b shows the same $c_{s,th}$ data plotted against the average $\chi$ ($\chi_{avg}$), where we assume that the interactions between solvent mixtures and polymers are volume-weighted averages of individual solvent–polymer interactions, *i.e.*, $\chi_{avg} = \varphi^S_{H_2O}\chi_{H_2O\text{-}p} + \varphi^S_{EG}\chi_{EG\text{-}p} + \varphi^S_{NMF}\chi_{NMF\text{-}p}$. The sharp maximum of $c_{s,th}$ in Fig. 1a can now be reasonably explained by the highest $\chi$ reflecting water–polymer interactions. In a related study, Li *et al.* compared the phase separation conditions[24] of two pairs of PECs with hydrophilic backbones (amide) and hydrophobic backbones (vinyl) and found that the latter has a $c_{s,th}$ at least 6 times as large as the former in water. Their study, though tuning the polymer–solvent interaction through a different approach, also underpinned the vital role of $\chi$ in dictating the associative phase separation of PECs.

Similarly, Lou *et al.* examined the effect of increasing local polarity through a polymer series with sulfide, sulfone and sulfoxide groups adjacent to cations and anions.[25] Using a sophisticated model, the authors observed $\chi$ values that progressively decrease with increasing molecular polarity (*i.e.*, better hydrophilicity) as extracted by fits to experimental binodal phase diagrams. Notably, their $\chi$ values obtained from fitting are largely in accord with estimated values in Table 2, perhaps lending some credence to estimates based on solubility parameters.

Table 2 Calculated effective $\chi_{solvent\text{-}p}$ values at room temperature

| $\chi_{solvent\text{-}p}$ | $H_2O$ | EG | NMF |
|---|---|---|---|
| PSS | 0.41 | 0.078 | 0.058 |
| PDADMA | 0.59 | 0.13 | 0.10 |
| Average | 0.50 | 0.10 | 0.080 |

## Application of the Voorn–Overbeek theory

In order to discern the source of the reduction of the critical salt concentration with decreasing $H_2O$, we use the Voorn-Overbeek (VO) theory.[43] While this model does not account for counterion binding, polymer connectivity, or dipole interactions, it allows us to determine if non-electrostatic interactions are primarily responsible for the non-monotonic behaviour. In VO theory, the single phase free energy density ($f$) of PEC solutions is

$$\frac{l^3 f\left(\varphi_p, \varphi_s\right)}{VkT} = \frac{\varphi_p}{N}\ln\left(\frac{\varphi_p}{2}\right) + \varphi_s \ln\left(\frac{\varphi_s}{2}\right) + \varphi_0 \ln \varphi_0 + \chi\varphi_p\varphi_0 - \alpha\left(\varphi_s + \sigma\varphi_p\right)^{\frac{3}{2}}. \quad (1)$$

In this equation, the first three terms represent the entropy of mixing of polymers, salts, and solvents. The fourth term

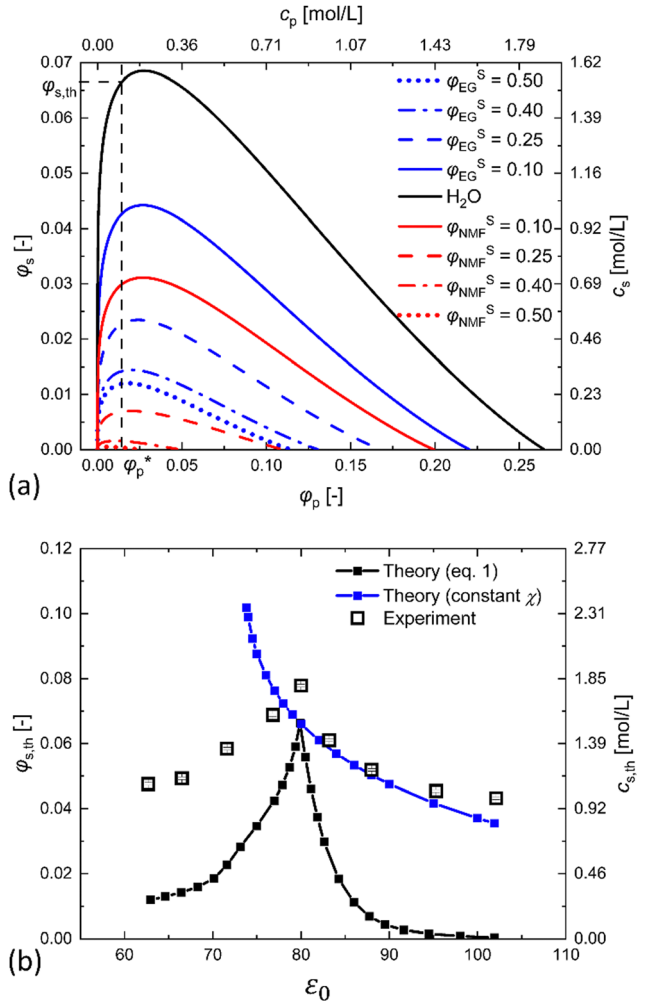


Fig. 2 (a) Theoretical $\varphi_s$–$\varphi_p$ phase diagrams calculated by VO theory in various solvent compositions. The $c_s$ axis is associated with $\varphi_s$ by $c_s = \varphi_s\rho_s/M_s$, and the $c_p$ axis is associated with $\varphi_p$ by $c_p = \varphi_p\rho_p/M_p$, where $\rho$ and $M$ are the density and molar masses of monomers. Here, we use $\rho_s$ = 2.75 g mL$^{-1}$ and $M_s$ = 119 g mol$^{-1}$ for KBr, and $\rho_p$ = 1.1 g mL$^{-1}$ and $M_p$ = 154 g mol$^{-1}$ to estimate the average of a PSS–PDADMA monomer pair with a 1 : 1 stoichiometry. The vertical dashed line indicates the experimental $c_p$ value of 0.10 mol L$^{-1}$, and its intersections with the coexistence curves define the theoretical $\varphi_{s,th}$ or $c_{s,th}$. (b) Comparison between theoretical and experimental $c_{s,th}$ at $c_p$ = 0.10 mol L$^{-1}$, plotted as a function of $\varepsilon_0$. Uncertainties in the measurement are provided in Table 1 and are typically smaller than the symbols.

represents the enthalpy of mixing from Flory–Huggins theory, and the last term represents the Debye–Hückel approximation of the total electrostatic free energy introduced by all charged moieties. Here, $\varphi_i$ is the volume fraction of component $i$, $l$ is the lattice size, $V$ is the system volume, $k$ is Boltzmann's constant, $T$ is the temperature, and $N$ is the reduced chain length. The strength of the electrostatic interactions is determined by $\alpha = (2\sqrt{\pi}/3)(l_B/l)^{3/2}$, where $l_B = e^2/4\pi\epsilon_o\varepsilon_0 kT$ is the Bjerrum length with an elementary charge ($e$) and permittivity of free space ($\epsilon_o$). The charge density ($\sigma$) is equal to the total polymer charge divided by $N$. To reduce complexity, polymers, salts, and solvents are each treated as a single species. In the case of the solvents, this is equivalent to assuming the relative volume fractions of the three solvents is the same in both phases. This assumption is reasonable given that the data in Fig. 1b nearly collapse on a single curve.

To apply this model, we use microscopic data from the experiments for parameterization rather than fitting the model to the experimental data. Therefore, the results are based on the model's underlying physics rather than its ability to fit the data. We define $l$ as the size of a water molecule (0.332 nm). We take $N$ = 1000 and $\sigma$ = 0.1 commensurate with the polymers. The values $\chi$ and $\varepsilon_0$ are the same as those used in Fig. 1b. Additional details of model parameterization can be found in the Section III of the ESI.†

The coexistence curves on the $\varphi_s$–$\varphi_p$ ($c_s$–$c_p$) plane were obtained by minimizing the total free energy, and the results are shown in Fig. 2a. As anticipated, all the phase boundaries have similar shapes. The theoretical $c_{s,th}$ at $c_p$ = 0.10 mol L$^{-1}$ are extracted from Fig. 2a *via* the intersection of the dashed line and the phase boundaries. These values are plotted in Fig. 2b together with the experimental $c_{s,th}$ for direct comparison. As can be seen in Fig. 2b, the VO theory semiquantatively reproduces the experimental trend of $c_{s,th}$ *vs.* $\varepsilon_0$ with a minimal set of microscopically defined parameters. To determine how non-electrostatic interactions affect this prediction, we also fix $\chi$ to be that of $H_2O$ and vary $\varepsilon_0$. As can be seen in Fig. 2b, this results in the monotonic dependence of $c_{s,th}$ on $\varepsilon_0$.

The agreement between experimental data and VO theory combined with the monotonic result once $\chi$ was fixed suggests that non-electrostatic interactions are primarily responsible for the non-monotonic behaviour in $c_{s,th}$. This result indicates that including counterion binding, connectivity of the polymer in electrostatics, dipolar interactions, preferential solvation,[44,45] local dielectric constants,[46–48] varying $\chi$ as a function of $\varphi_p$,[49] and treating each species independently[50–52] are not necessary to understand the source of non-monotonicity. However, the use of a more advanced theory[21,23,25,38,53–55] may be able to elevate the predictions from semiquantitative to fully quantitative, especially the plateauing of $c_{s,th}$ with increasing $\varphi_{NMF}^S$. Small-angle neutron scattering combined with a multicomponent random phase approximation theory was used to extract the three Flory–Huggins parameters among polymers and two solvents by Jia *et al.* on an LCST systems.[56,57] Such an approach within an appropriate theory may test the assumption of $\chi$ weighted by the cosolvent volume fraction.

### Effect of solvent mixtures on lower critical solution temperature

Fig. 3 shows the representative transmittance-$T$ curves of the KPSS–PDADMAB complex solutions in binary and ternary solvent mixtures. In all samples, liquid–liquid phase separation was observed upon heating, as evident by the drastic decrease in transmission. Such a universal LCST behavior across the entire solvent range[18,19,27] is likely driven by the stronger electrostatic interaction at higher $T$, embodied in the $l_B(T)$ of water, EG and NMF as increasing functions of $T$ (Fig. S5, ESI†). On the other hand, the temperature dependence of the hydrophobic interaction between polyelectrolytes and solvents as

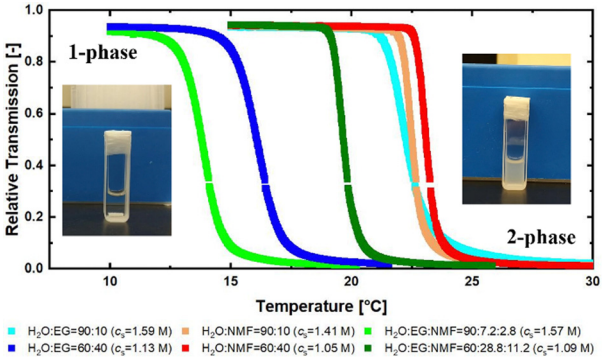


Fig. 3 Representative transmittance curves of KPSS–PDADMAB complexes in binary EG/$H_2O$, NMF/$H_2O$ and ternary EG/NMF/$H_2O$ mixtures with $c_p$ = 0.10 mol $L^{-1}$ and $c_s \approx c_{s,th}$, nearly identical to the conditions listed in Table 1. The inset figures are representative photographs of the same PEC solution in a DLS glass cuvette before (at low temperature) and after (above the LCST) phase separation.

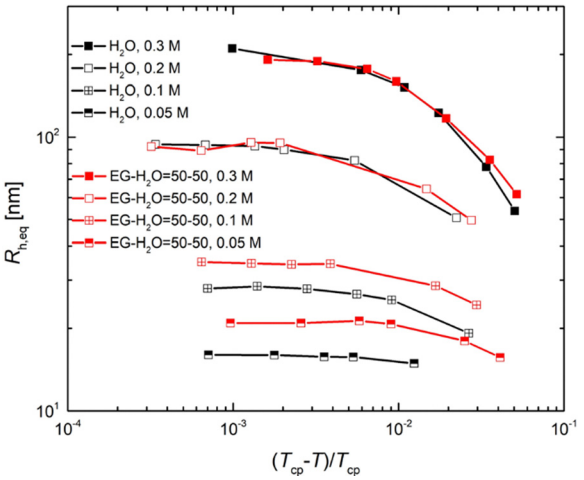


Fig. 4 Equivalent hydrodynamic radii ($R_{h,eq}$) of the polyelectrolyte complex aggregates in EG/$H_2O$ = 50/50 and pure water as a function of the thermodynamic distance, $(T_{cp} - T)/T_{cp}$. The solid lines connecting the data points are for visual aid. Uncertainties (error bars) are within the size of the symbols used and not shown, but were estimated by one standard deviation from the model fit to determine the diffusion coefficient and propagated to estimate the hydrodynamic radius using the Stokes–Einstein relationship.

represented by $\chi(T)$ has so far been poorly understood. Here, we introduced an empirical $\chi$ expression that includes both the enthalpic and entropic contributions following the formalism of the Flory–Huggins theory, *i.e.*, $\chi(T) = \chi_H/T + \chi_S$, and our simple model is able to capture an increase in critical salt concentration with increasing temperature through judicious parameterization of $\chi_H$ and $\chi_S$, which is consistent with the LCST behavior of PEC solutions up to 50% cosolvent volume fraction (as shown in Fig. S8 (ESI†), using $\chi_S \approx 4\ \chi_H/(293\ K)$ as an example). However, decreasing the entropic contribution of $\chi(T)$ can result in the reverse of the modelling results to UCST behaviors, due to the overwhelming miscibility of polyelectrolytes and solvents at high temperatures (as shown in Fig. S9 (ESI†), using $\chi_S = 0$ as an example). In the work by Adhikari *et al.*,[22] multiple phase behavior scenarios were also reported in aqueous PEC solutions, whereas in the present case, the trend based on the solvent mixtures is highlighted. The sensitivity in the choice of parameters ($\chi_H$ *vs.* $\chi_S$) reflects the complexity of these PEC systems and suggests the electrostatic–solvophobic competition as a possible mean-field mechanism for the dual miscibility gaps observed by Ye *et al.*[20] and predicted by Adhikari *et al.*[22] It is worth mentioning that the current knowledge on the criticalities of synthetic PECs is so far mostly established on the (Na/K)PSS–PDADMA(Cl/Br) systems and may therefore only stand for the case of hydrophobic backbones. From this sense, a systematic study of the temperature dependence of other model PEC systems of intermediate[25] or high backbone hydrophilicity[24] (and preferably, with low molar mass dispersity) would be beneficial to provide a general picture on this long-standing issue.

Apart from the temperature criticality and the phase diagrams,[18,19] we have also shown in our earlier study that upon approaching the critical temperatures, polycations and polyanions strongly associate with each other in water and eventually lead to concentration fluctuations of sub-micron size during incipient phase separation.[19,27] Therefore, it is also of interest to investigate whether such a chain association in mixed solvents is comparable with that in aqueous solution, or does it introduce new structures detectable by dynamic light scattering (DLS). Fig. 4 illustrates the trends in equivalent hydrodynamic radii ($R_{h,eq}$) of the polyelectrolyte chain associates at various $c_p$ with temperature in the case of the binary EG/$H_2O$ cosolvent with $\varphi^S_{EG}$ = 0.5. The horizontal axis here is $(T_{cp} - T)/T_{cp}$ rather than $T$ for the purpose of the direct comparison between the data, where $T_{cp}$ is the cloud point temperature of each individual sample as defined by the inflection points of transmittance-$T$ curves in Fig. 3. Therefore, the dimensionless $(T_{cp} - T)/T_{cp}$ denotes the thermodynamic distance of the experimental temperature to the phase separation temperature, nearly identical to the formalism of the Ginzburg criterion that is typically used to describe phase-separating charge-neutral systems. The polymer concentrations of 0.05 mol $L^{-1}$ to 0.30 mol $L^{-1}$ were selected to cover from dilute to semidilute solutions. Here, for clarity, we discuss the size of solution structures in the context of equivalent hydrodynamic radii, $R_{h,eq}$, while keeping in mind that the classical Stokes–Einstein relationship of $R_h = kT/6\pi\eta_0 D$ is only strictly valid in dilute solutions where all interparticle interactions are negligible with solvent viscosity, $\eta_0$.[27] Moreover, at temperatures that are sufficiently close to $T_{cp}$, the measured diffusion coefficients ($D$) given by DLS no longer represent the diffusion coefficients of individual particles or clusters, but instead the collective diffusion coefficients of concentration fluctuation modes as predicted by the mode-coupling theory.[58] This is beyond the scope of this paper but was addressed elsewhere.[27] Here, we do not distinguish the difference between the two but refer to the structures indiscriminately as associates. As can be clearly seen in Fig. 4, under all cases, the evolution of the chain association states in EG/$H_2O$ (red symbols and lines) display striking

similarities to that in pure water (black symbols and lines), with nearly overlapping curves for $c_p$ = 0.2 mol $L^{-1}$ and 0.3 mol $L^{-1}$, and only minor deviations for $c_p$ = 0.05 mol $L^{-1}$ and 0.1 mol $L^{-1}$ within experimental uncertainties on the logarithmic scale. Our results suggest that the effect of cosolvents does not change the dynamics of polyelectrolyte complexes, but only renormalizes their threshold salt concentrations and critical temperatures of phase separation.

## Conclusions

In conclusion, we observed a strong influence of cosolvents on the phase behaviour of KPSS/PDADMAB complexes, which displays non-monotonic dependence on the average dielectric constants of the binary or ternary solvent mixtures but can be reasonably interpreted by invoking a solvent–polymer backbone interaction term. The phase envelope shifts as a function of the cosolvent compositions were semiquantitatively captured by the VO model. While we expect that adding additional details would lead to more quantitative results, the simplicity of this model allows for a direct comparison of the importance of the electrostatic and non-electrostatic effects in describing this phenomenon. This model indicates that the van der Waals interactions are key to understanding the phase stability of coacervates in accord with our experimental findings. Moreover, within the broad composition window of cosolvents (EG–$H_2O$–NMF) used in this study, all PEC solutions manifest a universal LCST criticality, which is consistent with previous findings[18,19,27] and captured by the VO model as well by judicious parameterization. Further light scattering measurements lend credence on the similarity of the near-critical dynamics of PECs in aqueous and solvent mixtures. In all, our findings imply a novel way of tuning the phase stability of PEC solutions and may motivate fundamental studies in the fields such as biomedicines and cryo-preservation of cells, which also deal with similar circumstances where cosolvents are introduced to ensure solubility or proper functioning of proteins under harsh environments or processing conditions.

## Experimental

### Materials and polyelectrolyte complex sample preparation‡

Ethylene glycol (Fisher Scientific, certified grade) and *N*-methylformamide (Sigma-Aldrich, 99% purity) were used as received. Sodium poly(styrene sulfonate) (Sigma-Aldrich, nominal molar mass ≈200 kg $mol^{-1}$, 30% by mass fraction in $H_2O$) and poly(diallyl dimethylammonium chloride) (Sigma-Aldrich, nominal molar mass ≈(100 to 200) kg $mol^{-1}$, 20% by mass fraction in $H_2O$) were purified and counterion exchanged by previously reported methods. The number-average relative molar masses ($M_n$), dispersity ($Đ$), and degree of polymerization (DP) are summarized in Table 3.

Table 3 Characteristics of KPSS and PDADMAB

| Polyelectrolytes | $M_n$ (kg $mol^{-1}$) | $Đ$ | DP |
|---|---|---|---|
| KPSS | 70[a] | 2.80 | 315 |
| PDADMAB | 22[b] | 2.76 | 107 |

Note: [a] Relative number average molar mass determined by size exclusion chromatography (SEC) using NaPSS as calibrants. [b] Relative number average molar mass determined by SEC using poly(vinylpyrrolidone) as calibrants.

The dry KPSS and PDADMAB were individually dissolved in mixed solvents with predetermined ratios of ultrapure deionized water (Millipore), EG and NMF to prepare 0.50 mol $L^{-1}$ polymer stock solutions. The 2.00 mol $L^{-1}$ stock solutions or KBr were similarly prepared. The stock solutions of KPSS, PDADMAB and KBr were mixed with their corresponding blank solvents to prepare polyelectrolyte complex solutions with various salt concentrations ($c_s$). These complex solutions were vortex-mixed and vigorously agitated to ensure complete mixing and stored in a fridge at 5 °C to avoid solvent evaporation. The statuses of phase separation of the samples were determined by laser light transmittance measurements, with 50% transmittance as a criterion to distinguish between homogeneous and phase separation.

### Dielectric measurements

**Materials.** Anhydrous NMF and EG were obtained from Sigma Aldrich and used without further purification. Ultrapure water with a resistance reading of $>25$ MΩ was purified using a laboratory filtration and deionization unit. Concentration of mixtures was determined gravimetrically by weighing the content of pure components using a microbalance and then normalizing the mass fraction to volume fraction using the specific density of water (1.00 g $cm^{-3}$), NMF (1.110 g $cm^{-3}$) and EG (1.010 g $cm^{-3}$), respectively.

**Methods.** The static dielectric constant, $\varepsilon_0$, of pure solvents and their mixtures was determined from the measurements of complex dielectric permittivity ($\varepsilon^* = \varepsilon' - j\varepsilon''$) performed at 23 °C in a broadband frequency range from 400 MHz to 20 GHz. The measurements were performed using an Agilent 8720D Vector Network Analyzer and an Agilent 8570E Dielectric Probe Kit with an open-ended coaxial probe. The probe was impedance calibrated to open, short and water microwave impedance standards in accordance with the manufacturer specification for 8570E.

The example of the experimental data of $\varepsilon''(\omega)$ and $\varepsilon'(\omega)$ measured for NMF–$H_2O$ mixtures are plotted in Fig. 5a on the Cole–Cole $\varepsilon''$ *vs.* $\varepsilon'$ complex plane, where the angular frequency ($\omega$) is the independent parameter.

At higher frequencies, above 15 GHz, in the range where $\varepsilon'(\omega) < 40$ (Fig. 5a), the experimental $\varepsilon''$ and $\varepsilon'$ data are somewhat scattered due to effects of multiple reflections resulting from the dielectric compression of microwaves wavelength propagating in the high dielectric constant media. The plots

‡ Certain equipment, instruments, software, or materials are identified in this paper in order to adequately specify the experimental details. Such identification does not imply recommendation by the National Institute of Standards and Technology, nor does it imply the materials are necessarily the best available for the purpose. The symbols M used to represent mol $L^{-1}$ and are not in SI units, but used to adhere to the conventions of the journal.

 

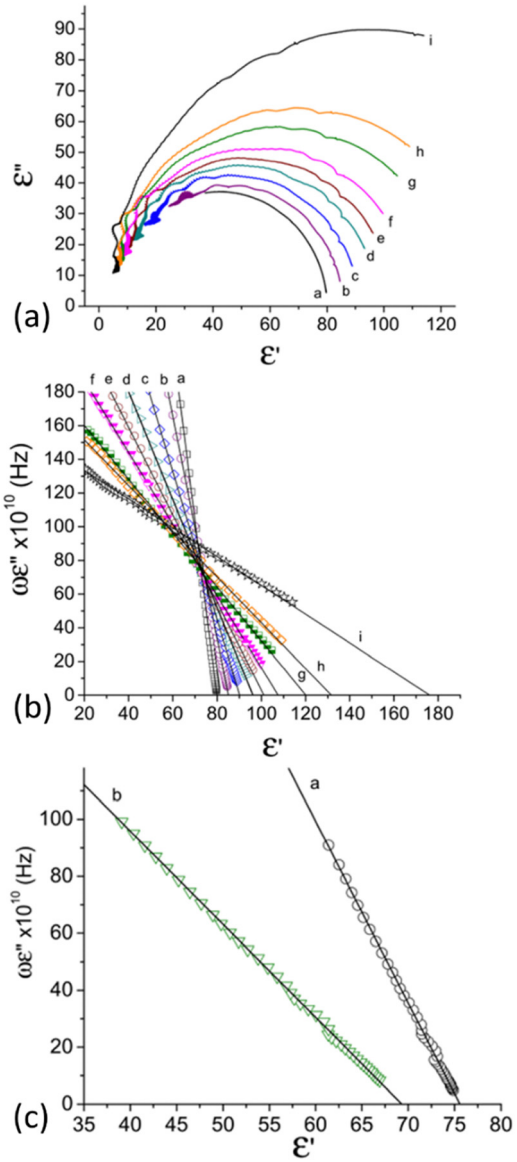


Fig. 5 (a) Cole–Cole representation of $\varepsilon''(\omega)$ *vs.* $\varepsilon'(\omega)$ for the NMF/$H_2O$ mixtures with the following NMF volume fractions: a – 0 (pure water), b – 16.7%, c – 36.9%, d – 48.7%, e – 59.2%, f – 67.2%, g – 78.2%, h – 85.0%, i – 100% (pure NMF). (b) Plots of $\omega\varepsilon''(\omega)$ *vs.* $\varepsilon'(\omega)$ for the same set of data in (a). (c) Plots of $\omega\varepsilon''(\omega)$ *vs.* $\varepsilon'(\omega)$ for EG/$H_2O$/NMF mixtures a-EG 17%, $H_2O$ 76%, NMF 6.8% with $\varepsilon_0$ = 75 and $\tau$ = 15 ps. b-EG 36%, $H_2O$ 52.4%, NMF 14.2% with $\varepsilon_0$ = 69 and $\tau$ = 30 ps. The solid lines represent linear fits to the data. Uncertainty information is provided in the ESI.†

in Fig. 5a show the apparent shape of Cole–Cole semi-circles that intersect $\varepsilon'(\omega)$ axis when $\varepsilon''(\omega)$ = 0. The two intersection points give the value of the unrelaxed dielectric constant, $\varepsilon_\infty(\omega \to \infty)$ and the static dielectric constant, $\varepsilon_0(\omega \to 0)$, which are parameters of the Cole–Cole relaxation model.[59]

In order to determine $\varepsilon_0$ from our empirical data, we can assume the single dielectric relaxation model of Debye for $\varepsilon''(\omega)$[59] described by,

$$\varepsilon''(\omega) = \frac{(\varepsilon_0 - \varepsilon_\infty)\omega\tau}{1 + \omega^2\tau^2} \quad (2)$$

where $\omega$ is the angular frequency, $\varepsilon''(\omega)$ is the imaginary part of the dielectric permittivity, and $\tau$ is the relaxation time.

Eqn (2) can be rearranged into (3):

$$\omega\varepsilon''(\omega) = \frac{1}{\tau}(\varepsilon_0 - \varepsilon'(\omega)) \quad (3)$$

which represents a linear relationship between the measured $\varepsilon''(\omega)$ and $\varepsilon'(\omega)$, The static dielectric constant, $\varepsilon_0$, is derived from (3) as the intercept of a straight line with the slope of $1/\tau$.

Fig. 5b and c show the plots of eqn (3) for mixtures of NMF/$H_2O$ and EG/NMF/$H_2O$, respectively, and the validity of eqn (3). Results for EG/$H_2O$ are shown in Section I, ESI.† Linear regression was performed on 400 data points. For clarity, only one symbol per 15 data points are plotted in Fig. 5b and c. The presented fitted lines support our assumption behind eqn (3), where the intercept of $\varepsilon'(\omega) = \varepsilon_0$ at $\omega$ = 0 has the physical meaning of the static dielectric constant.

### Laser transmittance

The laser transmittance measurement was performed using a homemade setup that includes a 532 nm wavelength solid state laser (Coherent VERDI), a set of neutral density filters, a sample heating stage with a Quantum Northwest TC125 temperature controller, and a Thorlabs PM100D power meter. The KPSS–PDADMAB complex solutions were transferred into rectangular glass cuvettes and placed in the heating stage. The relative transmittance was obtained by normalizing the transmitted laser power of the sample by that of the empty cuvette. During a temperature scan, the samples were heated at a rate of 0.5 °C $min^{-1}$ under constant stirring using a polytetrafluoroethylene stir bar, while the transmittance data as a function of time were recorded using the power meter software.

### Dynamic light scattering (DLS)

DLS measurements were performed using the same setup as described in the laser transmittance experiment, albeit with a single-mode fiber optic that collects the scattered light at $\theta$ = 90° with signal split to two photon counting modules (Excelitas Technologies) for cross-correlation measurement. Under the DLS mode, the scattered light intensities from filtered PEC samples as a function of time were monitored by the detector, recorded using the Brookhaven Windows 9kdlsw32 software, and simultaneously processed using a Brookhaven autocorrelator (TurboCorr) to give autocorrelation functions $g_2(\tau)$. This was then converted to the baseline-normalized first-order correlation function, $g_1(\tau)$, and fit to extract the decay rate $\Gamma$ following the protocol described previously (Fig. S10 and S11, ESI†).[27] Finally, $R_h$ was calculated using the Stokes–Einstein relationship assuming spherical particles: $R_h = kT/6\pi\eta_0 D = kTq^2/6\pi\eta_0\Gamma$, where $q$ is the scattering wave vector and $q = (4\pi n/\lambda)\sin(\theta/2)$ determined by the scattering angle ($\theta$), the refractive index of the solvent ($n$), and the wavelength ($\lambda$) of the incident light in a vacuum. The solvent viscosities ($\eta_0$) were estimated and are provided in Fig. S12 (ESI†).

## Data availability

The data supporting this article, including the calculation of the Flory–Huggins interaction parameters $\chi$, the parameterization of Voorn–Overbeek model, and the measurement results of solvent dielectric constants and dynamic light scattering, have been included as part of the ESI.†

## Conflicts of interest

There are no conflicts to declare.

## Acknowledgements

R. J. S. I. acknowledges partial support from the National Research Council – National Institute of Standards and Technology (NIST) Postdoctoral Fellowship Program. We acknowledge partial support from the NIST Materials Genome Initiative.

## Notes and references

1 R. J. Stewart, C. S. Wang, I. T. Song and J. P. Jones, *Adv. Colloid Interface Sci.*, 2017, **239**, 88–96.
2 M. M. Feldstein, E. E. Dormidontova and A. R. Khokhlov, *Prog. Polym. Sci.*, 2015, **42**, 79–153.
3 K. Sadman, D. E. Delgado, Y. Won, Q. Wang, K. A. Gray and K. R. Shull, *ACS Appl. Mater. Interfaces*, 2019, **11**, 16018–16026.
4 K. A. Black, D. Priftis, S. L. Perry, J. Yip, W. Y. Byun and M. Tirrell, *ACS Macro Lett.*, 2014, **3**, 1088–1091.
5 M. Muthukumar, *Macromolecules*, 2017, **50**, 9528–9560.
6 L. McQueen and D. Lai, *Front. Chem.*, 2019, **7**, 135.
7 H. Weingärtner, T. Merkel, U. Maurer, J.-P. Conzen, H. Glasbrenner and S. Käshammer, *Ber. Bunsen-Ges.*, 1991, **95**, 1579–1586.
8 N. C. Forero-Martinez, R. Cortes-Huerto, A. Benedetto and P. Ballone, *Molecules*, 2022, **27**, 1647.
9 J. Yu, N. E. Jackson, X. Xu, B. K. Brettmann, M. Ruths, J. J. de Pablo and M. Tirrell, *Sci. Adv.*, 2017, **3**, eaao1497.
10 N. E. Jackson, B. K. Brettmann, V. Vishwanath, M. Tirrell and J. J. de Pablo, *ACS Macro Lett.*, 2017, **6**, 155–160.
11 H. Falahati and A. Haji-Akbari, *Soft Matter*, 2019, **15**, 1135–1154.
12 C. E. Sing and S. L. Perry, *Soft Matter*, 2020, **16**, 2885–2914.
13 J. Fu and J. B. Schlenoff, *J. Am. Chem. Soc.*, 2016, **138**, 980–990.
14 V. S. Rathee, H. Sidky, B. J. Sikora and J. K. Whitmer, *J. Am. Chem. Soc.*, 2018, **140**, 15319–15328.
15 F. G. Quiroz and A. Chilkoti, *Nat. Mater.*, 2015, **14**, 1164–1171.
16 G. L. Dignon, W. Zheng, Y. C. Kim and J. Mittal, *ACS Cent. Sci.*, 2019, **5**, 821–830.
17 G. L. Dignon, R. B. Best and J. Mittal, *Annu. Rev. Phys. Chem.*, 2020, **71**, 53–75.
18 S. Ali, M. Bleuel and V. M. Prabhu, *ACS Macro Lett.*, 2019, **8**, 289–293.
19 Y. Ma, S. Ali and V. M. Prabhu, *Macromolecules*, 2021, **54**, 11338–11350.
20 Z. Ye, S. Sun and P. Wu, *ACS Macro Lett.*, 2020, **9**, 974–979.
21 S. Adhikari, M. A. Leaf and M. Muthukumar, *J. Chem. Phys.*, 2018, **149**, 163308.
22 S. Adhikari, V. M. Prabhu and M. Muthukumar, *Macromolecules*, 2019, **52**, 6998–7004.
23 A. S. Ylitalo, C. Balzer, P. Zhang and Z.-G. Wang, *Macromolecules*, 2021, **54**, 11326–11337.
24 L. Li, A. M. Rumyantsev, S. Srivastava, S. Meng, J. J. de Pablo and M. V. Tirrell, *Macromolecules*, 2021, **54**, 105–114.
25 J. Lou, S. Friedowitz, J. Qin and Y. Xia, *ACS Cent. Sci.*, 2019, **5**, 549–557.
26 Q. Wang and J. B. Schlenoff, *Macromolecules*, 2014, **47**, 3108–3116.
27 Y. Ma, S. D. Hudson, P. F. Salipante, J. F. Douglas and V. M. Prabhu, *ACS Macro Lett.*, 2023, **12**, 288–294.
28 R. Chollakup, W. Smitthipong, C. D. Eisenbach and M. Tirrell, *Macromolecules*, 2010, **43**, 2518–2528.
29 D. Priftis and M. Tirrell, *Soft Matter*, 2012, **8**, 9396–9405.
30 D. Priftis, X. Xia, K. O. Margossian, S. L. Perry, L. Leon, J. Qin, J. J. de Pablo and M. Tirrell, *Macromolecules*, 2014, **47**, 3076–3085.
31 P. K. Jha, P. S. Desai, J. Li and R. G. Larson, *Polymers*, 2014, **6**, 1414–1436.
32 G. R. Leader and J. F. Gormley, *J. Am. Chem. Soc.*, 1951, **73**, 5731–5733.
33 S. J. Bass, W. I. Nathan, R. M. Meighan and R. H. Cole, *J. Phys. Chem.*, 1964, **68**, 509–515.
34 A. Sehgal and T. A. P. Seery, *Macromolecules*, 1998, **31**, 7340–7346.
35 S. K. Filippov, T. A. P. Seery, P. Černoch, J. Pánek and P. Štěpánek, *Eur. Polym. J.*, 2011, **47**, 1410–1415.
36 S. K. Filippov, T. A. Seery, J. Kříž, M. Hruby, P. Černoch, O. Sedláček, P. Kadlec, J. Pánek and P. Štěpánek, *Polym. Int.*, 2013, **62**, 1271–1276.
37 G. Akerlof, *J. Am. Chem. Soc.*, 1932, **54**, 4125–4139.
38 P. Zhang, N. M. Alsaifi, J. Wu and Z.-G. Wang, *J. Chem. Phys.*, 2018, **149**, 163303.
39 S. Meng, Y. Liu, J. Yeo, J. M. Ting and M. V. Tirrell, *Colloid Polym. Sci.*, 2020, **298**, 887–894.
40 C. M. Hansen, *Hansen Solubility Parameters: A User's Handbook*, CRC Press, Boca Raton, 2nd edn, 2007.
41 D. W. Van Krevelen and K. Te Nijenhuis, *Properties of Polymers*, Elsevier, Amsterdam, 2009, 4th edn, pp. 189–227.
42 T. Lindvig, M. L. Michelsen and G. M. Kontogeorgis, *Fluid Phase Equilib.*, 2002, **203**, 247–260.
43 I. Michaeli, J. Overbeek and M. Voorn, *J. Polym. Sci.*, 1957, **23**, 443–450.
44 D. Mukherji, C. M. Marques and K. Kremer, *Nat. Commun.*, 2014, **5**, 4882.
45 X. Zhang, J. Zong and D. Meng, *Soft Matter*, 2020, **16**, 7789–7796.
46 Y. Wei, P. Chiang and S. Sridhar, *J. Chem. Phys.*, 1992, **96**, 4569–4573.
47 Z.-G. Wang, *Phys. Rev. E*, 2010, **81**, 021501.

 

48 I. Nakamura, A.-C. Shi and Z.-G. Wang, *Phys. Rev. Lett.*, 2012, **109**, 257802.
49 C. E. Sing and M. Olvera de la Cruz, *ACS Macro Lett.*, 2014, **3**, 698–702.
50 M. G. Cacace, E. M. Landau and J. J. Ramsden, *Q. Rev. Biophys.*, 1997, **30**, 241–277.
51 W. J. Xie and Y. Q. Gao, *J. Phys. Chem. Lett.*, 2013, **4**, 4247–4252.
52 M. Andreev, J. J. de Pablo, A. Chremos and J. F. Douglas, *J. Phys. Chem. B*, 2018, **122**, 4029–4034.
53 A. Salehi and R. G. Larson, *Macromolecules*, 2016, **49**, 9706–9719.
54 C. E. Sing, *Adv. Colloid Interface Sci.*, 2017, **239**, 2–16.
55 C. E. Sing and J. Qin, *Macromolecules*, 2023, **56**, 5941–5963.
56 D. Jia, T. Zuo, S. Rogers, H. Cheng, B. Hammouda and C. C. Han, *Macromolecules*, 2016, **49**, 5152–5159.
57 D. Jia, M. Muthukumar, H. Cheng, C. C. Han and B. Harnmouda, *Macromolecules*, 2017, **50**, 7291–7298.
58 R. A. Ferrell, *Phys. Rev. Lett.*, 1970, **24**, 1169–1172.
59 C. J. F. Böttcher, *Theory of electric polarization/Vol 2. Dielectrics in time-dependent fields*, completely revised by O. C. Van Belle, P. Bordewijk, and A. Rip., Elsevier, Amsterdam, 2nd edn, 1978.